

Scanning drift tube measurements of electron transport parameters in different gases: argon, synthetic air, methane and deuterium

I Korolov, M Vass and Z Donkó

Institute for Solid State Physics and Optics, Wigner Research Centre for Physics, Hungarian Academy of Sciences, 1121 Budapest, Konkoly Thege Miklós str. 29-33, Hungary

E-mail: donko.zoltan@wigner.mta.hu

Received 16 May 2016, revised 5 July 2016

Accepted for publication 20 July 2016

Published 13 September 2016



CrossMark

Abstract

Measurements of transport coefficients of electrons in a scanning drift tube apparatus are reported for different gases: argon, synthetic air, methane and deuterium. The experimental system allows the spatio-temporal development of the electron swarms ('swarm maps') to be recorded and this information, when compared with the profiles predicted by theory, makes it possible to determine the 'time-of-flight' transport coefficients: the bulk drift velocity, the longitudinal diffusion coefficient and the effective ionization coefficient, in a well-defined way. From these data, the effective Townsend ionization coefficient is determined as well. The swarm maps provide, additionally, direct, unambiguous information about the hydrodynamic/non-hydrodynamic regimes of the swarms, aiding the selection of the proper regions applicable for the determination of the transport coefficients.

Keywords: electron swarm, drift tube, transport coefficients

(Some figures may appear in colour only in the online journal)

1. Introduction

The transport coefficients of electrons in various gases are fundamentally important quantities and serve as principal input data of widely used fluid models of gas discharges. In addition, this—due to the fact that these coefficients can accurately be calculated from the cross section data—reliable transport coefficient data provide a possibility for checking/adjusting the electron-neutral collision cross section sets [1].

Throughout the past decades most of the transport coefficient data have been measured using *drift tube* apparatuses, in which low-density particle 'clouds' or 'swarms' are created and move under the effect of a homogeneous electric field. These systems have been based on different operating principles (photoelectric pulsed drift tubes, double-shutter drift tubes, systems based on photoionization of the gas, etc), see, e.g. [2–6]. As to the detection of the particles, in part of the

systems the displacement current generated in the electrode gap by the moving charges [7–9] is sensed, while in other systems the counting of particles arriving at a detector has been employed [3, 10, 11].

Notwithstanding the extensive work carried out in the past, interest in further drift tube measurements still persists. Experiments have been carried out recently for gases like CF_4 [12], CF_3I [13], and tetraethoxysilane [14], which have become important in processing applications. Other gases, like SF_6 , CF_3I , hydrofluoroolefine, $\text{He} + \text{H}_2\text{O}$ generated interest in swarm experiments because of their relevance to global warming, high voltage insulation, and biomedicine [15–18]. Particular transport effects [19–21] in specific gas mixtures (like negative differential conductivity) also motivate further experimental studies.

To obtain definite values of the transport coefficients it is important that measurements are conducted under

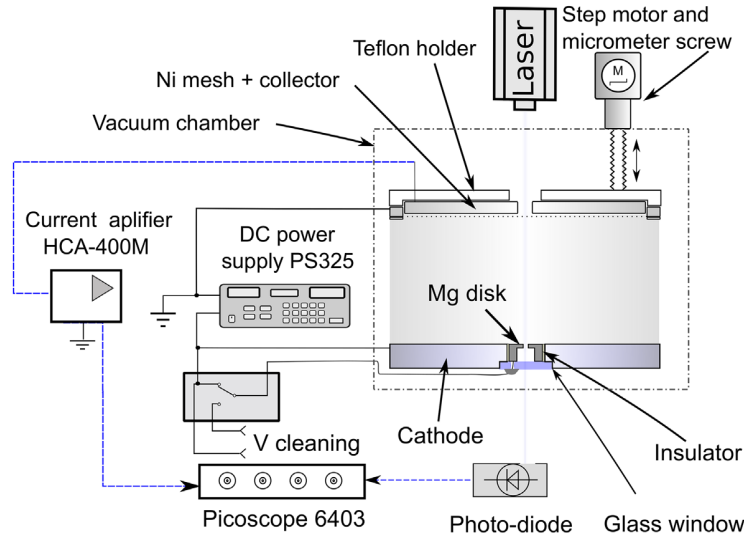


Figure 1. Simplified scheme of the experimental setup.

hydrodynamic conditions of the swarms, where the (reduced, i.e. density-rescaled) transport coefficients acquire unique values, which are functions only of the reduced electric field, E/N . In the hydrodynamic regime the space- and time-dependence of the electron density of a swarm generated at $t = 0$ and $z = 0$ is given as (see, e.g. [22]):

$$n_e(z, t) = \frac{n_0}{(4\pi D_L t)^{1/2}} \exp\left[\nu t - \frac{(z - Wt)^2}{4D_L t}\right], \quad (1)$$

where n_0 is the initial electron density, D_L is the (bulk) longitudinal diffusion coefficient, ν is the effective ionization frequency (equal to the ionization frequency minus the attachment frequency), and W is the *bulk drift velocity*, defined as

$$W = \frac{d}{dt} \left[\frac{\sum_{j=1}^{N_e(t)} z_j(t)}{N_e(t)} \right], \quad (2)$$

where $N_e(t)$ is the number of electrons in the swarm at time t . We note that it is important to distinguish the bulk drift velocity from the *flux drift velocity*, which is defined as

$$w = \frac{\sum_{j=1}^{N_e(t)} v_{j,z}(t)}{N_e(t)}, \quad (3)$$

because these two quantities acquire different values in the presence of non-conservative processes, like ionization and attachment (see, e.g. [23]).

It is clear from (1) that the evolution of the electron density of the swarm is governed by the bulk drift velocity, and therefore it is *this* velocity that is accessible in swarm experiments based on the measurement of quantities related to $n_e(z, t)$. The data acquisition procedures adopted in some experiments, however, yield velocities different from either of the (well-defined and well-understood) bulk and flux drift velocities (e.g. the so-called ‘mean-arrival time drift velocity’ [10])—the complexity of the interpretation of the measured

values has been discussed in detail, e.g. in [24] by Tagashira. (We note that in some publications no explicit reference is even given to the type of drift velocity values communicated.) In light of the above arguments, an ideal measurement and data acquisition approach should yield the bulk drift velocity, without any constraints on the effects of ionization/attachment and diffusion.

In [25] we have reported the development of a ‘*scanning*’ drift tube apparatus, which is capable of mapping the complete spatio-temporal evolution of electron swarms, developing between two plane electrodes (i.e. recording of ‘swarm maps’). This system operates with electron swarms initiated by photoelectron pulses and the spatio-temporal distribution of the electron flux is recorded while the electrode gap length (at a fixed electric field strength and gas density) is varied (see section 2). The mapping approach used in this system allows direct identification of the non-hydrodynamic and hydrodynamic regions, which is important because measurements taken in the latter are clearly required to obtain well-defined transport coefficients. As it will be shown later, the measurements allow a transparent determination of ‘time-of-flight’ transport parameters: the (bulk) *drift velocity* W , the (reduced) *longitudinal diffusion coefficient* ND_L , and the (reduced) effective ionization frequency ν/N , from a common data set measured at fixed conditions. From these coefficients we also derive the (reduced) *effective ionization coefficient* α/N , that characterizes the spatial growth of electron swarms under ‘steady-state Townsend’ conditions.

In section 2 of the paper the experimental apparatus and the data acquisition methods are described. Section 3 presents the experimentally determined transport coefficients, in comparison with those obtained in earlier works, for a number of gases: argon, synthetic air, methane and deuterium. Section 4 gives a brief summary of the work and an appendix provides the numerical values of the measured data.

2. Experimental apparatus and data evaluation

The simplified scheme of our experimental setup is shown in figure 1 and its concise description is given below. For a more complete description of the system the reader is referred to [25].

The drift cell is situated inside a stainless steel vacuum chamber (shown only in a simplified manner in figure 1) that is pumped down (by a turbomolecular pump backed by a rotary pump) to a base pressure of 10^{-5} Pa for several days preceding the measurements. During the experiments—that have been conducted at a temperature of $T = 293 \pm 2$ K—the gas pressure inside the chamber is measured by a Pfeiffer CMR 362 capacitive gauge. The gases, which flow through the chamber at a small flow rate of the order of 1–5 sccm (set by a mass flow controller), have at least 5.0 purity. In the case of deuterium the isotopic enrichment is $>99.8\%$.

Our drift tube operates in pulsed mode, bunches of photoelectrons are emitted (induced by $1.7 \mu\text{J}$ -energy pulses of a frequency-quadrupled diode-pumped YAG laser operated at ~ 3 kHz repetition rate) from a Mg disk embedded into the negatively biased stainless steel cathode, situated at the bottom of the drift cell. The cathode voltage is provided by a PS-325 (Stanford Research Systems) power supply. The laser light reaches the Mg disk via a quartz window of the top flange of the vacuum chamber and via a 5 mm hole drilled into the top electrode. The Mg disk has a 0.6 mm-diameter hole to allow part of the laser light to be detected by a fast photodiode placed underneath the cell, outside the vacuum chamber. The signal of this photodiode triggers the data collection.

A 105 mm-diameter stainless steel, virtually grounded collector electrode is situated at the top of the cell. An electrically grounded nickel grid with $T = 88\%$ transmission and 45 lines/inch density is mounted at a fixed distance of 1 mm in front of the collector electrode. The collector and the grid are moved together by a stepping motor-driven micrometer screw mounted on a vacuum feedthrough of the vacuum chamber (see figure 1). The distance between the emitter (cathode) and the grid can be set within the range of $L = 13.6$ – 63.6 mm (we use 0.2–1 mm step size to map the development of the swarm). The electrodes are electrically insulated from the grounded chamber wall with Teflon sheaths.

In pulsed drift tubes equipped with only two electrodes ('pulsed Townsend' setup) the displacement current generated by all the charge carriers moving in the inter-electrode gap is sensed [7], which is proportional to the spatial integral of the electron density $n_e(z, t)$ (provided that the particle transport is hydrodynamic). In our system, the signal at the collector, $I(z, t)$, is also generated by the displacement current, which is however, induced only by the electrons that enter the field free grid-collector gap. The contribution of any electron upon entering this region to the current signal generated at the collector is proportional to its velocity. At low pressures these electrons fly through this narrow (1 mm) gap quickly, while at high pressures their velocity becomes quickly randomized due to collisions. In

either case the duration of the current pulse generated by a single incoming electron is very short. The superposition of a high number of such pulses generated by a high number of electrons entering the grid-collector gap is fed to a high speed current amplifier (type Femto HCA-400M) and is measured, synchronized with the photo-diode signal, by a digital oscilloscope (type Picoscope 6403B) with 0.8 ns time resolution.

The measured signal can be assumed to be proportional to the *flux* of the electrons entering the grid-collector gap. It follows that, as in the hydrodynamic regime the flux and the density are proportional, in this domain our system senses the $n_e(z, t)$ density of the swarm, given by (1). Accordingly, the data shown in the form of 'swarm maps' in the next section can be interpreted as the electron density. (Note that the effect of the motion of ions is neglected due to the short time scales of interest here.)

The experiment is controlled by a computer using LabView software in sequential measurements. During the mapping sequence, the voltage is continuously adjusted to ensure that E/N remains fixed for the different gap sizes. Data obtained for 3000–5000 pulses (depending on the signal intensity) are averaged at each position of the collector.

Scanning the electrode separation and recording the collector current allows us to obtain complete information about the *spatial and temporal evolution of the electron swarms*. The recording time of a swarm map, with an acceptable signal to noise ratio, takes typically ≈ 25 – 100 min.

The values of W , D_L , and ν can be obtained by fitting the function (1)—that includes these parameters—to the measured $I(z, t)$ data. In the fitting procedure, care has to be taken to limit the fitting region where hydrodynamic transport prevails, i.e. the swarm is fully equilibrated beyond a transient region near the source [26]. In our previous work [25] we have shown that the transient region—if present within the domain accessible in the measurements—is clearly observable in the swarm maps.

Having determined the 'time-of-flight' transport coefficients W , D_L , and ν , the effective Townsend ionization coefficient, α , which is characteristic for steady-state Townsend experiments, is calculated as:

$$\frac{1}{\alpha} = \frac{W}{2\nu} + \sqrt{\left(\frac{W}{2\nu}\right)^2 - \frac{D_L}{\nu}}, \quad (4)$$

based on the discussions in the papers of Tagashira [27] and of Blevin and Fletcher [28]. In the absence of diffusion (i.e. $D_L = 0$) equation (4) reduces to $\alpha = \nu/W$. This value is increased in the presence of diffusion, for the gases and conditions covered here this increase is between less than 1% and 20%.

Besides the fitting of the whole theoretical and measured density distribution we also apply a 'slicing' method as another way to determine the bulk drift velocity. Cutting the $I(z, t)$ maps of the swarm, or the $n_e(z, t)$ density of the swarm, given by (1), at *fixed values of time* results in symmetrical, Gaussian functions, and the peaks of these functions can

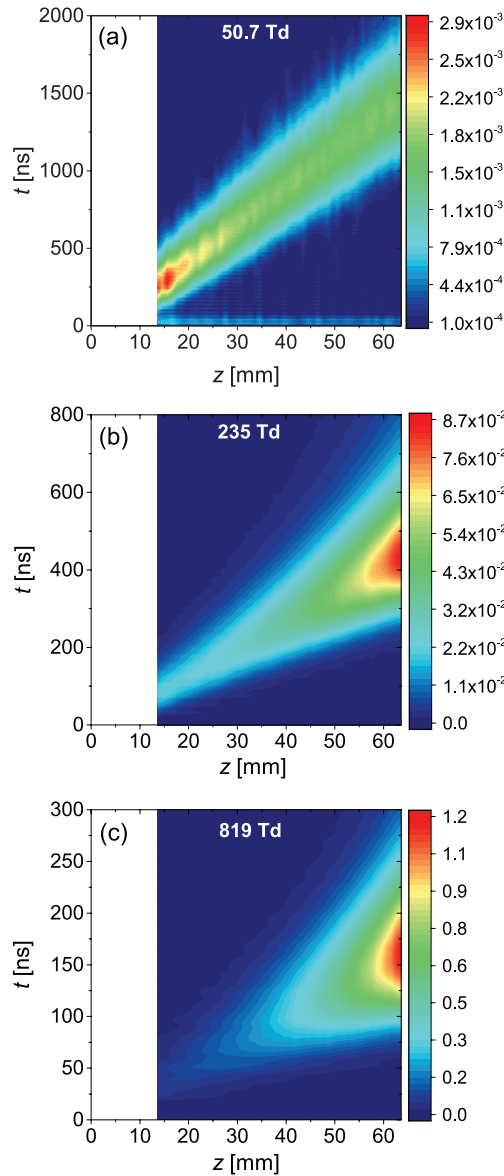


Figure 2. Swarm maps recorded in argon gas at reduced electric fields of (a) 50.7 Td, (b) 235 Td and (c) 819 Td. Note the different time domains covered by the vertical axes. The color scales represent electron density and are given in arbitrary units, which are, however, the same for all panels.

be associated with the center-of-mass of the particle cloud. A straight line fit to the measured peak position as a function of time gives the value of W directly (for more details see [25]).

The spatio-temporal distribution of the density of the swarm as given by (1) does not take into account transverse diffusion, which, however, is present in the experiment and can have an effect on the results under conditions when particles get lost at the cell wall (i.e. not all electrons arrive at the collector). To ensure that this effect—which may become important at long gaps—is not significant, we have executed the fitting of the measured signals to the theoretical form (1) for different subdomains of z and compared the resulting transport coefficients. The results were accepted and are presented here only

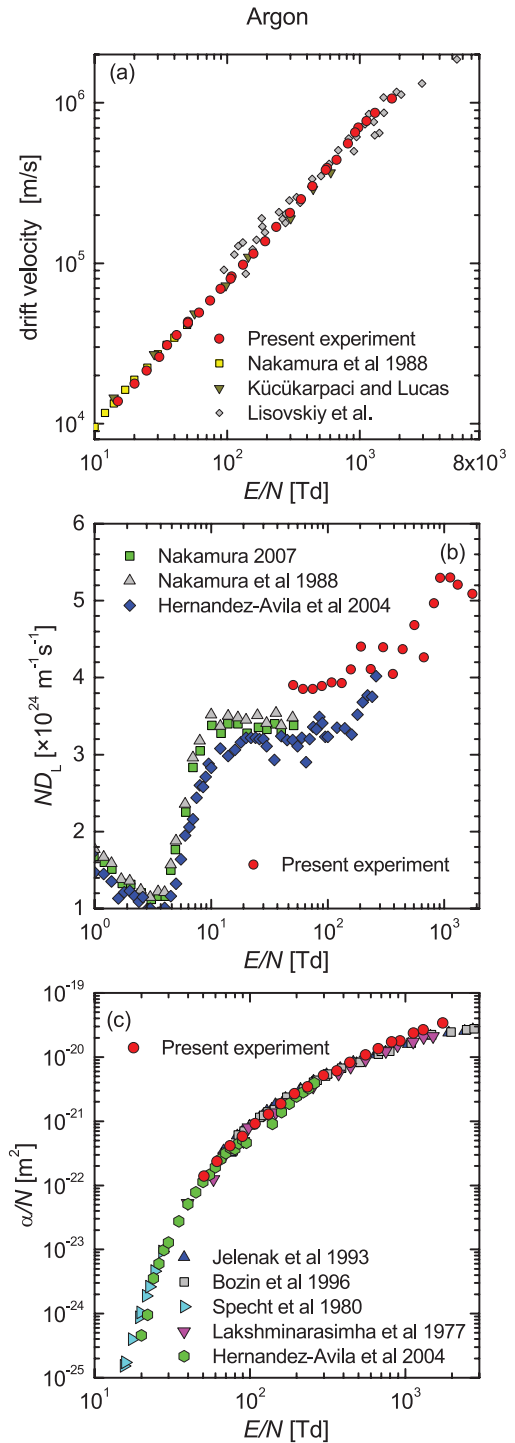


Figure 3. Electron transport coefficients in argon: (a) drift velocity, (b) reduced longitudinal diffusion coefficient and (c) reduced ionization coefficient. Previous data: Nakamura and Kurachi [29], Küçükarpaci and Lucas [30], Lisovskiy *et al* [31], Nakamura [32], Hernández-Ávila *et al* [33], Jelenak *et al* [34], Bozin *et al* [35], Specht *et al* [36], Lakshminarasimha and Lucas [37]. Panel (a) [25] reprinted with permission AIP Publishing LLC. Copyright 2016 AIP Publishing LLC.

for those cases when the deviations between the data obtained from the fits over different z domains were within $\pm 3\%$ for W , $\pm 5\%$ for D_L and ν ($\pm 10\%$ for synthetic air, due to the worse signal to noise ratio, see later).

3. Results

In the following we present the experimental results for the different gases: argon, synthetic air, methane and deuterium. For each gas, representative examples are first given for the spatio-temporal swarm maps, and subsequently, we present the measured transport coefficients, in comparison with previous experimental data. We recall again that in previous works the definitions of the measured velocities differ and in some cases it is not even clear what kind of velocity was determined in a given experiment. Therefore we label the vertical axes of the corresponding figures as ‘drift velocity’ and discuss in the text the definitions used by the different authors, whenever this is possible.

For the determination of the bulk drift velocity W we use both the slicing method and the fitting of the measured data to the theoretical $n_e(z, t)$ profiles, described above. We find that at low E/N the first method gives more accurate data, while at high E/N , where only a part of the Gaussian distributions is recorded, the fitting method has a better performance. (At low and medium E/N values the two methods were found to yield drift velocities differing not more than 1%.) For the determination of the longitudinal diffusion coefficient and the effective ionization frequency only the fitting of the complete distributions is used. Besides the graphical presentation of W , ND_L and α/N , numerical values of these coefficients are also given in an appendix. The appendix contains as well values of ν/N , which are not presented in the figures.

The accuracy of the transport coefficients is mainly limited by the noise present in the swarm maps (as will also be visible in the examples of $I(z, t)$ presented). At good signal to noise ratio the stability of the system ensured accurate reproducibility of the data, e.g. drift velocity values measured at the same conditions but on different days did not differ more than 2%. The estimated errors of the results will be given at their presentation.

3.1. Argon

Exemplary spatio-temporal maps of electron swarms in argon gas are presented in figure 2, for different values of the reduced electric field, covering the range $E/N \sim 50$ Td ... 800 Td. At the lowest electric field traces of the equilibration of the swarm (as quasi-periodic structures) are observable at small gaps. At this low field (50.7 Td) ionization is negligible and the spatial spreading of the electron cloud is rather low, indicating a small value of D_L . A relatively high noise, characteristic of weak signals, measured, e.g. in the absence of appreciable ionization, is also seen here. At the higher electric fields the electron density grows significantly with the distance from the electron source, indicating the onset of significant ionization. At the higher fields ($E/N = 235$ Td and 819 Td) the maps confirm that the swarms are already equilibrated within the non-accessible range of gap lengths ($z \leq 13.6$ mm). At the highest E/N the amplitude of $I(z, t)$ reaches about 3 orders of magnitude higher values as compared to those recorded at the lowest E/N .

The electron transport coefficients in argon gas are presented in figure 3. Our data for the measured bulk drift velocity of electrons, W —which cover a broader range of E/N compared to any of the previous studies—agree well with those given by Nakamura and Kurachi [29] and Küçükarpaci and Lucas [30] at lower E/N values and with the data of Lisovski *et al* [31] at higher E/N (see figure 3(a)). We note that the latter data were derived from the radiofrequency breakdown characteristic of argon and not in a drift tube experiment, and have comparatively large scattering, unlike our data, which have an estimated error smaller than 3% for $E/N \leq 1000$ Td, and $\sim 5\%$ at $E/N > 1000$ Td.

The longitudinal diffusion coefficient D_L is presented in figure 3(b) together with values measured by Nakamura [32] in a double shutter drift tube below 50 Td, using a UV photoelectric source, results obtained by Nakamura and Kurachi [29] in a double shutter drift tube employing a filament electron source, as well as data provided by Hernández-Ávila *et al* [33] from measurements on a pulsed Townsend apparatus operated with UV (N_2 , 337 nm) laser pulses, covering a broader range of the reduced electric field, up to $E/N = 400$ Td. Our data extend the previously available values up to $E/N \approx 1000$ Td, however, the scattering of the data is higher compared to the case of the drift velocity, as the fitting of D_L is more susceptible to the noise of the measured data. This results in an accuracy of $\pm 10\%$ for our data for D_L . Between $E/N = 50$ Td and 200 Td our measurements indicate a $\approx 20\%$ higher diffusion coefficient compared to the data of [33] (where a typical error of D_L was claimed to be 10–15%).

The present values of the reduced ionization coefficient are shown in figure 3(c) in comparison with the data of Jelenak *et al* [34] and Bozin *et al* [35] who obtained the ionization and excitation coefficients for a wide range of the reduced electric field, 50 Td–9 kTd, via measurements of the spatial dependence of the optical emission intensity from a stationary Townsend discharge (operated in the μA regime); Specht *et al* [36] who deduced the ionization coefficient from the ratio of the integrated ion and electron currents in a pulsed drift-tube apparatus, and Lakshminarasimha and Lucas [37] who obtained α/N under stationary conditions, between 8 and 1271 Td, based on the measurements of the current as a function of electrode gap in a drift tube. Our measured values (of which the accuracy we estimate to be below 6%) cover a wider range of E/N , compared to the previous studies.

3.2. Synthetic air

Among all the gases, the lowest signal intensities and, consequently, the worst signal to noise ratios were found for synthetic air, most likely due to the modification of the photoelectron yield of the Mg disk by the gas itself. To achieve acceptable signal intensities the surface of the Mg disk had to be cleaned regularly by a sputtering discharge in Ar gas, which was possible using a separate electrical connection to the disk that could be connected as cathode without opening the vacuum chamber (for more details see [25]). This procedure resulted only in temporary enhancement of the signal, making it possible to measure up to five swarm maps with acceptable signal to noise ratio.

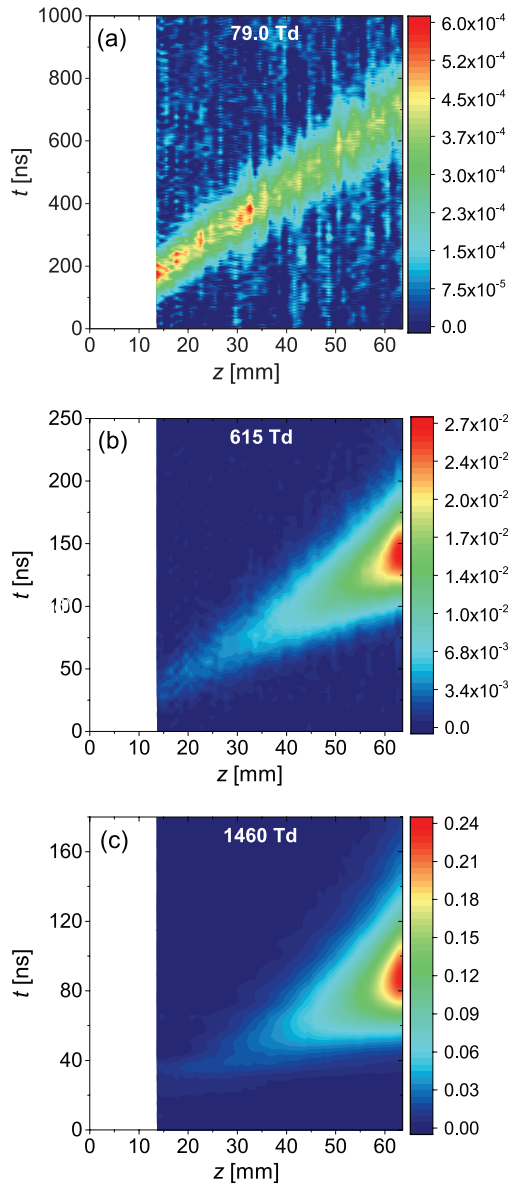


Figure 4. Swarm maps recorded in synthetic air, at reduced electric fields of (a) 79 Td, (b) 615 Td and (c) 1460 Td. Note the different time domains covered by the vertical axes. The color scales represent electron density and are given in arbitrary units, which are, however, the same for all panels.

The poor signal to noise ratio is well visible in the swarm map recorded at the low value of $E/N = 79$ Td, see figure 4(a). With increasing E/N the signal to noise ratio improves, but the quality of the data is still inferior compared to the other gases, which finally makes the determination of the transport parameters, especially the diffusion and ionization coefficients, less accurate and the results are limited to the high E/N range.

The obtained values of the electron drift velocity in synthetic air are presented in figure 5(a). This figure includes data originating from several previous studies as well, that cover different domains of E/N . (Note that most of these previous measurements have been carried out using dry, but not

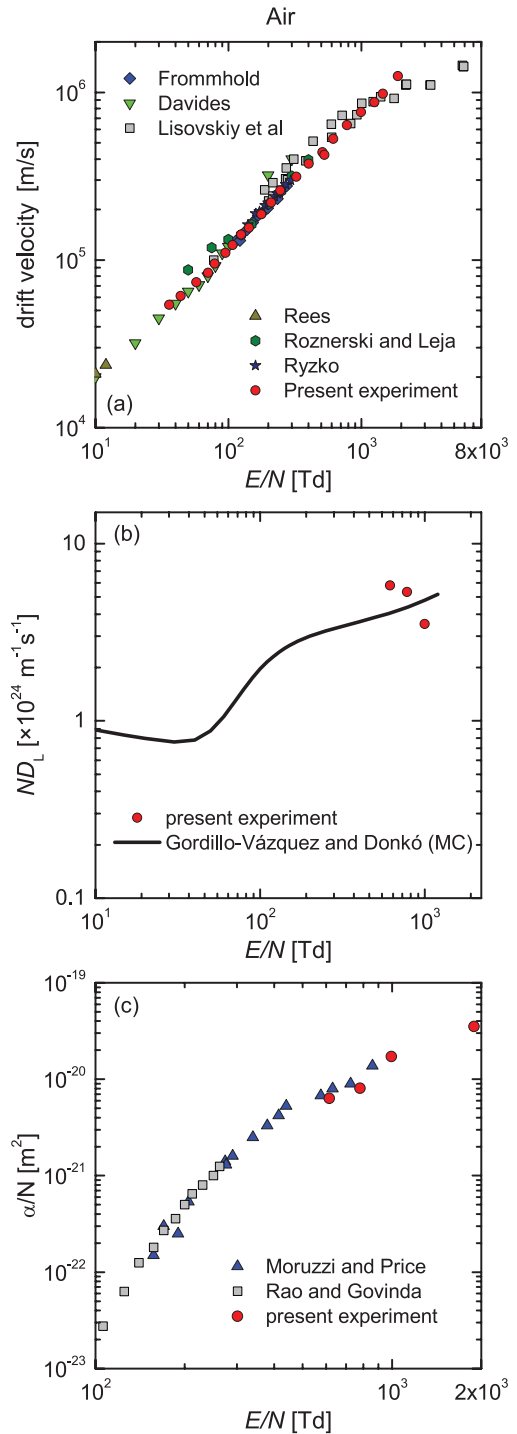


Figure 5. Electron transport coefficients in synthetic air: (a) drift velocity, (b) reduced longitudinal diffusion coefficient and (c) reduced effective ionization coefficient. Previous experimental and simulation data: Rees [38], Davies [39], Frommhold [40], Ryzko [41], Roznerski and Leja [42] and Lisovskiy and Yegorenkov [43], Gordillo-Vázquez and Donkó [46].

synthetic air. Minor constituents of dry air are, however, not expected to result in a significant change of the drift velocity.) The present data cover a wider domain of the reduced electric field than any of the previous works. All data sets agree

reasonably well. At low E/N the agreement with the data of Rees [38] and Davies [39] is quite good, as well as at medium E/N values (between 100 Td and 300 Td) with the data of Frommhold [40] and Ryzko [41]. Roznerski and Leja [42] used a double shutter time-of-flight setup for measuring the drift velocity for E/N between 0.6 to 250 Td. The data of Lisovskiy and Yegorenkov [43] show comparatively more scattering, but we note, that as in the case of argon (see above), that their data were derived from the radiofrequency breakdown characteristic of the gas.

Experimental data for the longitudinal diffusion coefficient in air are difficult to find in the literature. Most studies have focused on the determination of the transverse diffusion coefficient only, see [44, 45] and references therein. Therefore, in figure 5(b) we include a simulation result for D_L obtained in [46], for comparison with our present data. Due to the weak signals in the experiment only a few data points (having an error up to $\pm 15\%$) are given in figure 5(b) for D_L . For other (i.e. lower E/N) conditions even higher uncertainties were found and therefore the data are not presented.

The poor signal to noise in synthetic air also hindered the determination of the effective ionization coefficient in our measurements, data are only given for $E/N > 600$ Td. Nevertheless, the data agree reasonably with the values of α/N obtained in previous experiments of Raja Rao and Govinda Raju [47] as well as that of Moruzzi and Price [48], both based on measurements of the growth of a photoeffect-initiated current with gap length of their drift tubes. The uncertainty of our data for α/N is less than 10%.

3.3. Methane

The widest range of E/N with good signal to noise ratio was reached in methane, our measurements in this gas cover values from 1.5 Td to ~ 1500 Td. Illustrative examples of the measured swarm maps are shown in figure 6. At low E/N (figure 6(a)) the map indicates a negligible ionization and slow diffusion, the signal is concentrated within a narrow domain in space and time, i.e. the cloud practically does not spread while it travels with a well-defined velocity. For the case of the medium E/N of 118 Td (figure 6(b)) we find a decreasing peak intensity of the signal with increasing time and position, which is caused by the spreading of the electron cloud, due to the increased rate of diffusion at low ionization rate. At the highest reduced electric field of 1520 Td we see the onset of ionization, there is a strong increase of the signal intensity as a function of position (see figure 6(c)).

The transport coefficients derived from the $I(z, t)$ swarm maps are displayed in figure 7 as a function of E/N , in comparison with data provided in earlier works. For comparison we include data from the following works. Al-Amin *et al* [49] used the TOF technique with a fixed drift gap length to obtain the drift velocity and the longitudinal diffusion coefficient within the range 0.28–848 Td; Davies *et al* [50] determined the transport coefficients of electron swarms initiated by UV light illumination, in a drift tube with variable gap length; Hunter

et al [51] provided data for the drift velocity and the effective ionization coefficient using the pulsed Townsend technique; Schmidt and Roncossek [6] used two-photon ionization by intense UV laser light within the gas phase to create electron swarms and determined the drift velocity, as well as D_L and D_T , at low reduced electric fields, limited to $E/N \leq 15$ Td; Berghöfer *et al* [5] used as well UV laser ionization in the gas phase, however, in this experiment two laser beams were used to ionize the gas at two different positions, and the difference between the arrival times of the two particle clouds were measured; Yoshida *et al* [11] employed a double shutter drift tube and measured the arrival time ‘spectrum’ of electrons. The results obtained in all these experiments show a high degree of consistency, and a good agreement is also found with our present data, especially for the drift velocity values shown in figure 7(a). With regards to the longitudinal diffusion coefficient (see figure 7(b)) our data are most consistent with those of Al-Amin *et al* [49]: we find a $\sim 15\%$ higher minimum value for D_L at around 50 Td compared to Yoshida *et al* [11], from whose values we also find deviations at E/N values exceeding 200 Td—in this higher E/N range our values are closest to those given by Al-Amin *et al* [49]. With regards to the effective ionization coefficient our measurements indicate slightly higher values as compared to other works around $E/N \sim 100$ Td. At high E/N values our data agree the best with Davies *et al* [50] and are 10–15% lower than those given by Yoshida *et al* [11]. The uncertainties of the present values for ND_L and α/N , are below 8% and 6%, respectively.

3.4. Deuterium

Examples of recorded swarm maps for deuterium are shown in figure 8, while the transport coefficients are given in figure 9. We have also experienced for this gas a relatively poor signal to noise ratio at low E/N , which, however, improved significantly towards higher reduced electric fields.

Our drift velocity data are compared to the results of previous studies in figure 9(a). Petrović and Crompton [52] covered the 3–30 Td range of the reduced electric field and determined the drift velocity from the transit time of the swarm in a double shutter type drift tube. Roznerski *et al* [53] measured the drift velocity in a double shutter drift tube in the range of 3–125 Td. Values for low reduced electric fields ($E/N < 15$ Td) were also given by McIntosh [54]. While at low E/N all data sets agree well, the present experiments indicate a noticeably higher drift velocity above ~ 30 Td, compared to the data of Roznerski *et al* [53]. For E/N values below 400 Td the estimated error of our data for the drift velocity is below 3%, and for high E/N this grows up to 6%.

The solid line labelled as ‘Roznerski *et al* (calc)’ in figure 9(a) was given in [53] as a result of a two-term solution of the Boltzmann equation with the cross sections by Buckman and Phelps [55]. While in [53] it was concluded that this cross section set may need to be adjusted, our present results are in a very good agreement with this calculated curve.

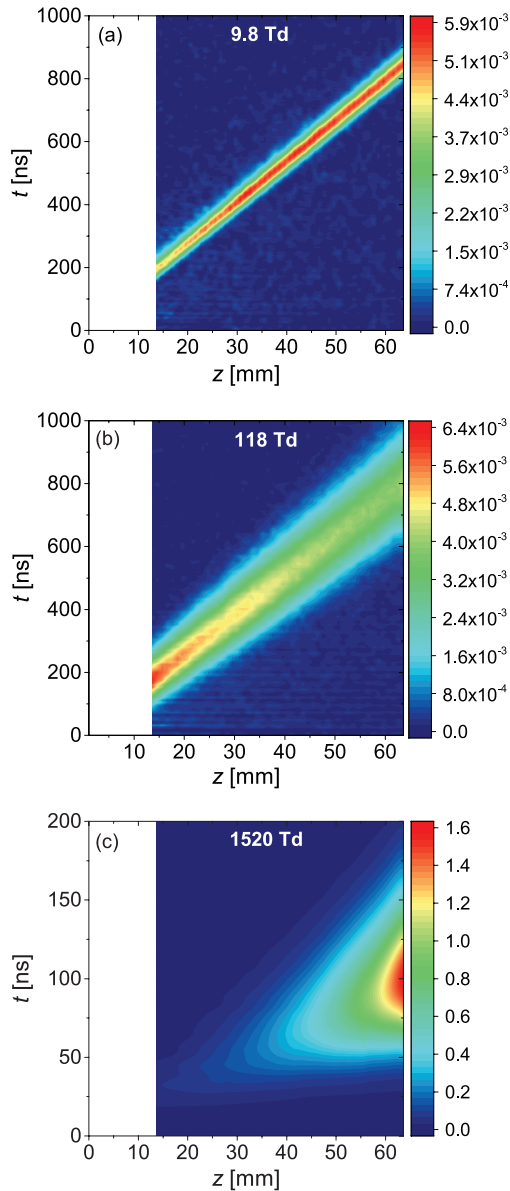


Figure 6. Swarm maps recorded in methane, at reduced electric fields of (a) 9.8 Td, (b) 118 Td and (c) 1520 Td. Note the different time domains covered by the vertical axes. The color scales represent electron density and are given in arbitrary units, which are, however, the same for all panels.

We were able to find values for the longitudinal diffusion coefficient of electrons in D_2 only in the paper of McIntosh [54] (for low reduced electric fields, $E/N < 6$ Td). This set of data, together with the values measured in the present experiment are displayed in figure 9(b). The reduced ionization coefficient as a function of E/N , in comparison with values obtained by other authors is presented in figure 9(c). The data of Rose [56], Cowling and Fletcher [57], as well as Davies *et al* [58] were obtained via measurements of current growth in drift tubes with variable gap lengths. All data sets for α/N , including ours, agree reasonably well over the whole domain of E/N . The error of our data for $D_L N$ and α/N is estimated to be less than 10%.

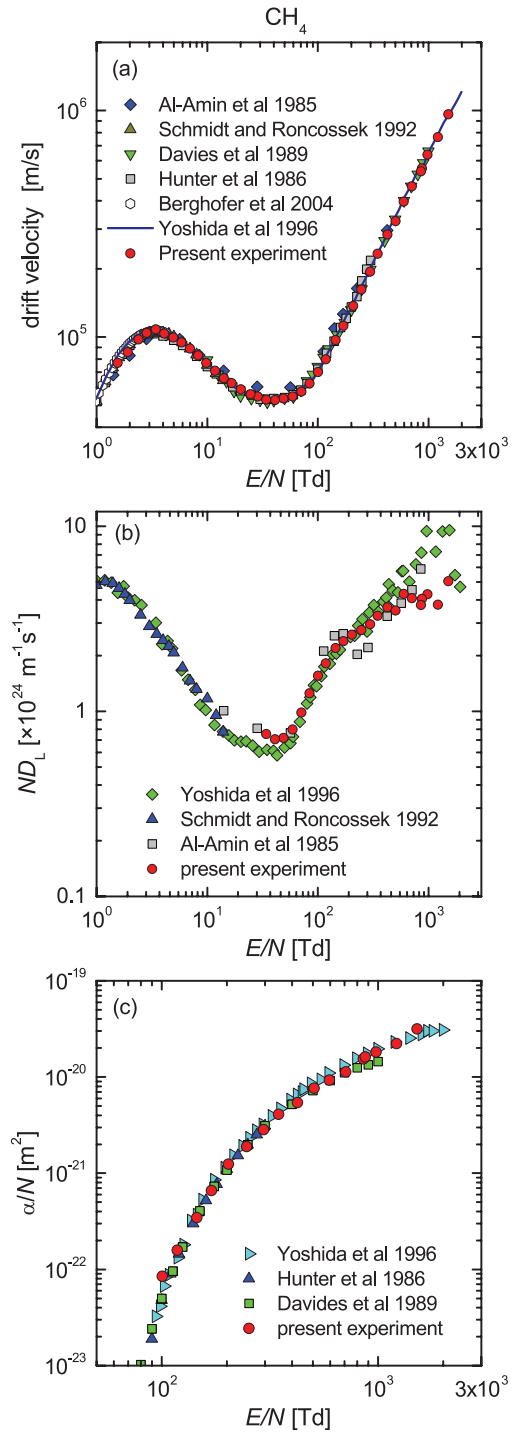


Figure 7. Electron transport coefficients in methane: (a) drift velocity, (b) reduced longitudinal diffusion coefficient and (c) reduced effective ionization coefficient. Previous data: Al-Amin *et al* [49], Davies *et al* [50], Hunter *et al* [51], Schmidt and Roncossek [6], Berghöfer *et al* [5], Yoshida *et al* [11].

4. Summary

A scanning drift tube apparatus, capable of mapping the complete spatial and temporal development of electron swarms has been employed to determine transport coefficients (bulk

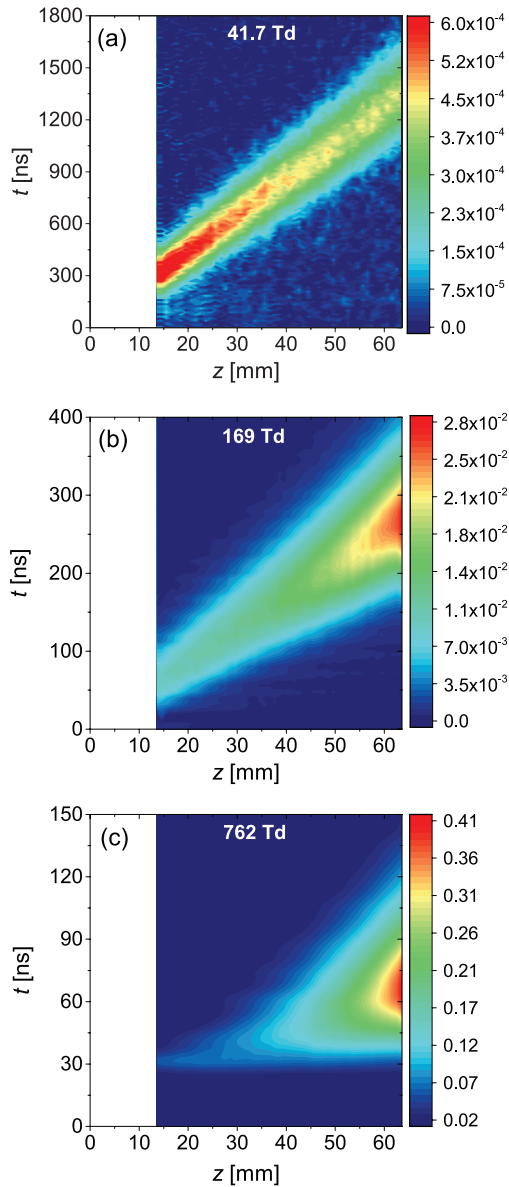


Figure 8. Swarm maps recorded in deuterium, at reduced electric fields of (a) 41.7 Td, (b) 169 Td and (c) 762 Td. Note the different time domains covered by the vertical axes. The color scales represent electron density and are given in arbitrary units, which are, however, the same for all panels.

drift velocity, longitudinal diffusion coefficient, the effective ionization frequency and Townsend ionization coefficient) of electrons in different gases: argon, synthetic air, methane and deuterium. All three transport coefficients have been determined from the measured spatial and temporal distributions of the electron density, under hydrodynamic conditions, which are directly confirmed by the measured data, making calculations of the equilibration processes unnecessary. The transport coefficients determined in our experiments are given below in tabulated form in the appendix.

Our measurements have covered a wider range of E/N , or extended it (typically to higher E/N values) compared to most of the previous investigations. For some conditions the poor signal to noise ratio has hindered the accurate determination

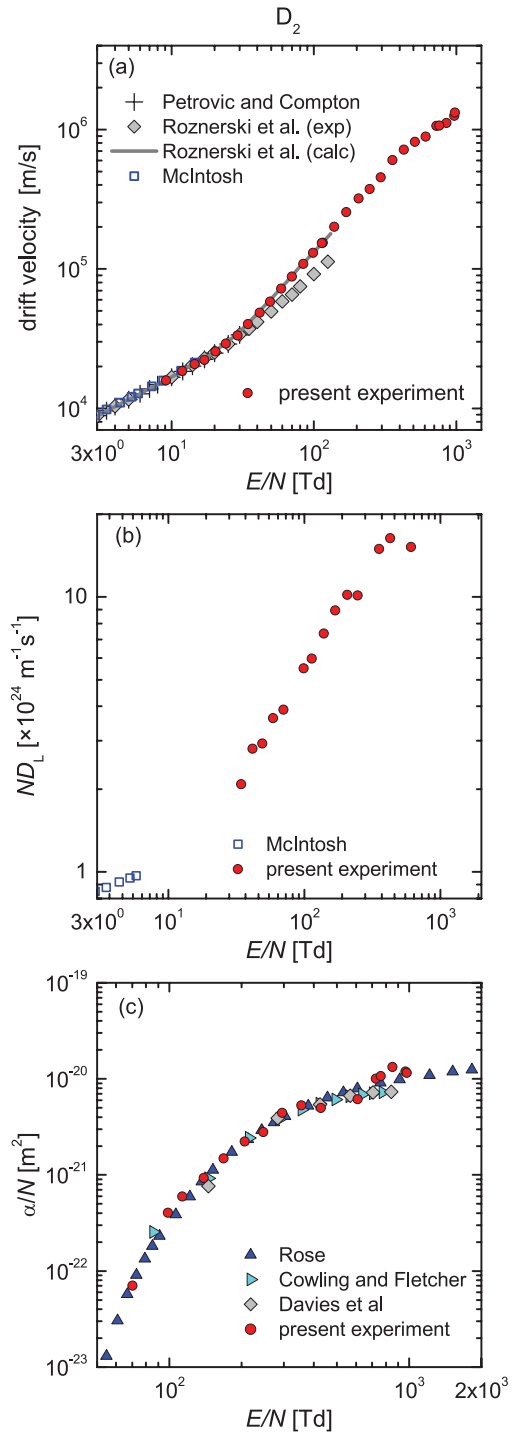


Figure 9. Electron transport coefficients in deuterium: (a) drift velocity, (b) reduced longitudinal diffusion coefficient and (c) reduced ionization coefficient. Previous data: Petrović and Crompton [52], Roznerski *et al* [53], McIntosh [54], Rose [56], Cowling and Fletcher [57], Davies *et al* [58].

of the transport coefficients (especially D_L), application of a higher power UV laser source and/or a better electron emitter material could enhance the capabilities of our instrument. As an additional extension the collector electrode can be re-designed to consist of electrically separated rings, allowing the determination of the transverse diffusion coefficient, D_T , as well.

Table A1. Measured electron bulk drift velocity in different gases at 293 K, as a function of the reduced electric field.

Argon		Synthetic air		Methane		Deuterium	
E/N (Td)	W (10^4 m s $^{-1}$)	E/N (Td)	W (10^4 m s $^{-1}$)	E/N (Td)	W (10^4 m s $^{-1}$)	E/N (Td)	W (10^4 m s $^{-1}$)
15.01	1.38	36.01	5.40	1.552	7.70	9.155	1.59
20.05	1.78	43.81	6.10	1.919	8.61	11.93	1.86
24.74	2.15	57.54	7.35	2.397	9.77	14.52	2.08
30.78	2.61	70.39	8.40	2.835	10.44	17.03	2.24
35.31	3.09	78.99	9.50	3.426	10.84	20.32	2.57
41.54	3.57	94.89	11.0	4.107	10.37	24.15	2.92
50.75	4.23	107.6	12.3	4.944	9.98	29.08	3.34
61.41	4.93	124.9	14.2	5.883	9.50	34.41	4.04
74.73	5.87	143.3	15.6	6.978	8.93	41.65	4.87
89.38	6.92	177.1	18.7	8.310	8.32	49.30	5.85
106.5	8.03	209.8	22.0	9.700	7.71	59.10	7.26
108.4	8.30	245.9	26.0	11.76	7.12	70.27	8.83
131.9	9.79	325.3	31.4	14.19	6.59	84.17	10.9
158.6	11.5	403.3	37.5	16.61	6.28	98.82	13.1
193.8	13.7	510.5	43.9	20.12	5.90	113.8	15.4
235.3	16.8	528.6	42.3	24.72	5.60	115.9	15.5
298.7	20.7	614.6	52.8	28.62	5.49	139.2	20.1
362.8	25.1	781.1	63.7	34.24	5.31	168.7	25.7
440.7	30.3	996.5	76.1	40.98	5.29	206.5	32.1
554.8	38.2	1260	87.4	48.86	5.37	246.4	37.5
569.0	39.3	1459	98.0	59.18	5.48	295.8	45.7
670.9	44.1	1889	125	71.05	5.76	356.0	60.5
818.6	55.9			84.09	6.26	429.2	71.9
926.5	65.6			100.8	7.02	513.0	82.0
979.2	70.1			118.3	7.99	609.8	89.3
1129	77.0			145.3	9.71	726.0	106
1308	86.8			170.2	11.3	762.7	107
1750	106			208.8	13.8	852.6	112
				246.9	16.2	966.9	126
				296.5	19.5	978.6	133
				346.83	23.4		
				424.8	28.4		
				505.8	32.6		
				596.5	39.7		
				708.6	46.4		
				854.2	54.0		
				872.4	55.7		
				978.6	64.1		
				1219	76.4		
				1516	96.6		

Acknowledgments

This work was supported by the Hungarian Fund for Scientific Research (OTKA), via grant K105476. We gratefully acknowledge the contributions of T Szűcs and P Hartmann to the development of the experimental apparatus. We thank N Pinhão and D Loffhagen for useful discussions.

Appendix

The tables A1–A4 below give numerical values of the electron transport coefficients obtained in our measurements.

References

- [1] Petrović Z Lj, Šuvakov M, Nikitović Ž, Dujko S, Šašić O, Jovanović J, Malović G and Stojanović V 2007 *Plasma Sources Sci. Technol.* **16** S1
- [2] Elford M T 1972 *In Case Studies in Atomic and Collision Physics* vol 2, ed E W McDaniel and M R C McDowell (Amsterdam: North-Holland) ch 2
- [3] Huxley L G H and Crompton R W 1974 *The Diffusion and Drift of Electrons in Gases* (New York: Wiley)
- [4] Crompton R W 1994 *Advances in Atomic, Molecular and Optical Physics* vol 33, ed M Inokuti (New York: Academic)
- [5] Berghöfer Th, Blümer J and Hörandel J R 2004 *Nucl. Instrum. Methods Phys. A* **525** 544

Table A2. Measured reduced longitudinal diffusion coefficient of electrons in different gases at 293 K, as a function of the reduced electric field.

Argon		Synthetic air		Methane		Deuterium	
E/N (Td)	ND_L ($10^{24} \text{ m}^{-1} \text{ s}^{-1}$)	E/N (Td)	ND_L ($10^{24} \text{ m}^{-1} \text{ s}^{-1}$)	E/N (Td)	ND_L ($10^{24} \text{ m}^{-1} \text{ s}^{-1}$)	E/N (Td)	ND_L ($10^{24} \text{ m}^{-1} \text{ s}^{-1}$)
50.75	3.91	614.6	5.79	34.24	0.755	34.41	2.09
61.41	3.86	781.1	5.33	40.98	0.709	41.65	2.81
74.73	3.85	996.5	3.52	48.86	0.719	49.30	2.94
89.38	3.89			59.19	0.800	59.10	3.63
108.4	3.94			71.10	0.986	70.27	3.90
131.9	3.93			84.09	1.25	98.82	5.51
158.6	4.11			100.8	1.56	113.3	5.97
193.8	4.40			118.3	1.82	139.2	7.38
235.3	4.11			145.3	2.20	168.7	8.94
298.7	4.40			170.2	2.40	206.5	10.2
362.8	4.05			203.9	2.60	246.4	10.2
440.7	4.37			246.9	2.76	355.9	15.0
554.8	4.68			296.5	2.97	429.2	16.4
670.8	4.27			346.8	3.29	609.8	15.3
818.6	4.97			424.8	3.67		
926.5	5.30			505.8	3.51		
1129	5.30			596.5	4.31		
				708.6	4.10		
				854.2	3.76		
				872.4	4.06		
				978.6	4.30		
				1219	3.77		
				1516	5.07		

Table A3. Measured reduced effective ionization frequency in different gases at 293 K, as a function of the reduced electric field.

Argon		Synthetic air		Methane		Deuterium	
E/N (Td)	ν/N ($10^{-14} \text{ m}^3 \text{ s}^{-1}$)	E/N (Td)	ν/N ($10^{-14} \text{ m}^3 \text{ s}^{-1}$)	E/N (Td)	ν/N ($10^{-14} \text{ m}^3 \text{ s}^{-1}$)	E/N (Td)	ν/N ($10^{-14} \text{ m}^3 \text{ s}^{-1}$)
24.74	0.00002	614.6	0.307	100.8	0.0006	70.27	0.0006
30.78	0.00006	781.1	0.445	118.3	0.0013	98.82	0.0051
35.31	0.00011	996.5	1.21	145.3	0.0033	113.3	0.0091
41.54	0.00025	1889	3.65	170.2	0.0074	139.2	0.0174
50.75	0.00059			203.9	0.017	168.7	0.035
61.41	0.0014			246.9	0.030	206.5	0.067
74.75	0.0024			296.5	0.053	246.4	0.097
89.38	0.0039			346.8	0.090	295.8	0.185
108.4	0.0073			424.8	0.142	355.9	0.282
131.9	0.012			505.8	0.228	429.2	0.318
158.6	0.020			596.5	0.332	609.8	0.468
193.8	0.034			708.6	0.450	726.0	0.940
235.3	0.053			854.2	0.698	762.6	0.995
298.7	0.095			872.4	0.761	852.6	1.28
362.8	0.139			978.6	0.973	966.9	1.36
440.7	0.220			1219	1.38	978.6	1.35
554.8	0.371			1516	2.56		
670.8	0.518						
818.6	0.817						
926.5	1.08						
1129	1.53						

Table A4. Measured reduced Townsend ionization coefficient in different gases at 293 K, as a function of the reduced electric field.

Argon		Synthetic air		Methane		Deuterium	
E/N (Td)	α/N (10^{-20} m ²)						
24.74	0.0007	614.6	0.64	100.8	0.009	70.27	0.007
30.78	0.0023	781.1	0.81	118.3	0.016	98.82	0.041
35.31	0.0036	996.5	1.72	145.3	0.035	113.3	0.060
41.54	0.0070	1889	3.51	170.2	0.067	139.2	0.094
50.75	0.014			203.9	0.125	168.7	0.150
61.41	0.024			246.9	0.191	206.5	0.225
74.75	0.038			296.5	0.286	246.4	0.281
89.38	0.058			346.8	0.413	295.8	0.445
108.4	0.091			424.8	0.544	355.9	0.531
131.9	0.128			505.8	0.771	429.2	0.500
158.6	0.188			596.5	0.937	609.8	0.618
193.8	0.267			708.6	1.14	726.0	1.01
235.3	0.345			854.2	1.55	762.6	1.07
298.7	0.519			872.4	1.63	852.6	1.33
362.8	0.614			978.6	1.82	966.9	1.20
440.7	0.825			1219	2.24	978.6	1.16
554.8	1.08			1516	3.18		
670.8	1.35						
818.6	1.73						
926.5	1.79						
1129	2.38						

- [6] Schmidt B and Roncossek M 1992 *Aust. J. Phys.* **45** 351
- [7] Raether H 1964 *Electron Avalanches and Breakdown in Gases* (London: Butterworths)
- [8] de Urquijo J, Arriaga C A, Cisneros C and Alvarez I 1999 *J. Phys. D: Appl. Phys.* **32** 41
- [9] Dahl D A, Teich T H and Franck C M 2012 *J. Phys. D: Appl. Phys.* **45** 485201
- [10] Kondo K and Tagashira H 1990 *J. Phys. D: Appl. Phys.* **23** 1175
- [11] Yoshida K, Ohshima T, Ohmori Y, Ohuchi H and Tagashira H 1995 *J. Phys. D: Appl. Phys.* **29** 1209
- [12] Dengming X and Yunkun D 2013 *Plasma Sources Sci. Technol.* **15** 25
- [13] de Urquijo J, Juárez A M, Basurto E and Hernández-Ávila J L 2007 *J. Phys. D: Appl. Phys.* **40** 2205
- [14] Yoshida K, Ohshima T, Ohuchi H, Kishimoto Y and Tagashira H 1996 *J. Phys. D: Appl. Phys.* **29** 2447
- [15] Christophorou L G and Olthoff J K 2000 *J. Phys. Chem. Ref. Data* **29** 267
- [16] de Urquijo J, Mitrani A, Ruiz-Vargas G and Basurto E 2011 *J. Phys. D: Appl. Phys.* **44** 342001
- [17] Chachereau A, Rabie M and Franck C M 2016 *Plasma Sources Sci. Technol.* **25** 045005
- [18] de Urquijo J, Basurto E, Juárez A M, Ness K F, Brunger M J and White R D 2014 *J. Chem. Phys.* **141** 014308
- [19] Šašić O, de Urquijo J, Juárez A M, Dupljanin S, Jovanović J, Hernández-Ávila J L, Basurto E and Petrović Z Lj 2010 *Plasma Sources Sci. Technol.* **19** 034003
- [20] de Urquijo J 2002 *Plasma Sources Sci. Technol.* **11** A86
- [21] Dyatko N A, Kochetov I V and Napartovich A P 2014 *Plasma Sources Sci. Technol.* **23** 043001
- [22] Robson R E 1991 *Aust. J. Phys.* **44** 685
- [23] Dujko S, White R D and Petrović Z Lj 2008 *J. Phys. D: Appl. Phys.* **41** 245205
- [24] Tagashira H 1992 *Aust. J. Phys.* **45** 365
- [25] Korolov I, Vass M, Bastykova N Kh and Donkó Z 2016 *Rev. Sci. Instrum.* **87** 063102
- [26] Malović G, Strinić A, Živanov A, Marić D and Petrović Z Lj 2003 *Plasma Sources Sci. Technol.* **12** S1
- [27] Donkó Z 2011 *Plasma Sources Sci. Technol.* **20** 024001
- [28] Tagashira H, Sakai Y and Sakamoto S 1977 *J. Phys. D: Appl. Phys.* **10** 1051
- [29] Blevin H A and Fletcher J 1984 *Aust. J. Phys.* **37** 593
- [30] Nakamura Y and Kurachi M 1988 *J. Phys. D: Appl. Phys.* **21** 718
- [31] Küçükarpaci H N and Lucas J 1981 *J. Phys. D: Appl. Phys.* **14** 2001
- [32] Lisovskiy V A 1998 *Tech. Phys. Lett.* **24** 308
- [33] Lisovskiy V, Booth J-P, Landry K, Douai D, Cassagne V and Yegorenkov V 2006 *J. Phys. D: Appl. Phys.* **39** 660
- [34] Nakamura Y 2007 *Proc. of 28th ICPIG* pp 224–6
- [35] Hernandez-Avila J L, Basurto E and de Urquijo J 2004 *J. Phys. D: Appl. Phys.* **37** 3088
- [36] Jelenak Z M, Velikić Z B, Božin J V, Petrović Z Lj and Jelenković B M 1993 *Phys. Rev. E* **47** 3566
- [37] Božin J V, Jelenak Z M, Velikić Z V, Belča I D, Petrović Z Lj and Jelenković B M 1996 *Phys. Rev. E* **53** 4007
- [38] Specht L T, Lawton S A and DeTemple T A 1980 *J. Appl. Phys.* **51** 166
- [39] Lakshminarasimha C S and Lucas J 1977 *J. Phys. D: Appl. Phys.* **10** 313
- [40] Rees J A 1973 *Aust. J. Phys.* **26** 427
- [41] Davies D K 1983 *Theoretical Notes, Note 346* (Pittsburgh, PA: Westinghouse RD Center)
- [42] Frommhold L 1963 *Fortschr. Phys.* **12** 597
- [43] Ryzko H 1965 *Proc. Phys. Soc. Lond.* **85** 128
- [44] Roznerski W and Leja K 1984 *J. Phys. D: Appl. Phys.* **17** 279
- [45] Lisovskiy V A and Yegorenkov V D 1998 *J. Phys. D: Appl. Phys.* **31** 3349
- [46] Rees J A and Jory R L 1971 *Aust. J. Phys.* **17** 307
- [47] Raja Rao C and Govinda Raju G R 1971 *J. Phys. D: Appl. Phys.* **4** 769
- [48] Gordillo-Vázquez F J and Donkó Z 2009 *Plasma Sources Sci. Technol.* **18** 034021

- [47] Raja Rao C and Govinda Raju G R 1971 *J. Phys. D: Appl. Phys.* **4** 494
- [48] Moruzzi J L and Price D A 1974 *J. Phys. D: Appl. Phys.* **7** 1434
- [49] Al-Amin S A J, Küçükarpacı H N and Lucas J 1985 *J. Phys. D: Appl. Phys.* **18** 1781
- [50] Davies D K, Kline L E and Bies W E 1989 *J. Appl. Phys.* **65** 3311
- [51] Hunter S R, Carter J G and Christophorou L G 1986 *J. Appl. Phys.* **60** 24
- [52] Petrović Z Lj and Crompton R W 1992 *Aust. J. Phys.* **42** 609
- [53] Roznerski W, Mechlińska-Drewko J, Leja K and Petrović Z Lj 1994 *J. Phys. D: Appl. Phys.* **27** 2060
- [54] McIntosh A I 1966 *Aust. Phys.* **19** 805
- [55] Buckman S J and Phelps A V 1985 *J. Chem. Phys.* **82** 4999
- [56] Rose D J 1956 *Phys. Rev.* **104** 273
- [57] Cowling I R and Fletcher J 1973 *J. Phys. B: At. Mol. Phys.* **6** 665
- [58] Davies D E, Smith D and Myatt J 1961 *Proc. V Int. Conf. Ion Phenom. in Gases (Munich)* vol 1 p 678